# Field Analysis of New Coaxial Dielectrometer

Weiguo Xi and Wayne R. Tinga, *Member, IEEE*

*Abstract*—**In response to the new developments in high temperature microwave dielectrometers, [1], [2] a field analysis of a composite sample insertion hole in a coaxial re-entrant cavity is performed via a mode-matching formulation. In this paper, the formulation and the numerical method are presented. The numerical results are discussed with attention focused on the hole effects on the dielectric loaded cavity. By virtue of this analysis and the structure which allows for the sample insertion holes, a new dielectrometer is obtained featuring both ease of sample insertion and accuracy in dielectric determinations. This paper demonstrates that solid, liquid or powdered samples can be readily accommodated and measured, and the dielectric data obtained via two theoretically calculated calibration curves are in good agreement with published data.**

## I. Introduction

CAVITY perturbation methods have been widely used to measure complex permittivities of materials at microwave frequencies [3]–[5]. These measurements are conducted by introducing a small, properly shaped sample into a cavity and determining its dielectric properties from the shift in the cavity's resonant frequency and the drop in its quality factor. In order to introduce the sample into a cavity without opening the cavity each time, it is convenient to have a hole in one endplate. Such a sample insertion hole can also ensure testing repeatability, easy sample preparation and elimination of the typical air gap problem [6], [7]. However, this hole also leads to a field redistribution, which in turn produces uncertainties in dielectric determinations if the effect of the hole is not taken into account.

The hole in a cavity causes a departure from a simple idealized cavity geometry and makes it exceedingly difficult to obtain exact field solutions. Only a few authors have given an analysis of the hole effect, mainly on cylindrical cavities [8]–[10]. Recent progress in the development of new high temperature microwave dielectrometers and applicators requires the analysis of hole effects on the coaxial re-entrant cavity with a hollow center conductor [1], [2]. Our experiments have shown that a cavity with insertion holes has significantly different sample loading effects compared to a cavity without holes [1].

In this paper, the mode-matching formulation and the numerical method for analyzing electromagnetic fields in the composite hole are presented. Effects of the hole on resonant frequency and Q-factor are discussed in detail. An error analysis for dielectric determinations is also included. Finally, complex dielectric data for a number of well-characterized materials are presented as obtained from two calculated calibration curves which include effects of both the insertion hole and the sample holder.

Manuscript received July 30, 1991; revised March 12, 1992.

The authors are with the Electrical Engineering Department, University of Alberta, Edmonton AB, Canada T6G 2G7.

IEEE Log Number 9202138.

## II. Formulation and Numerical Method

### A. Structure

The geometry of the cavity analyzed in this paper is depicted in Fig. 1(a). Unlike ordinary coaxial re-entrant cavities, this cavity has a hollow center conductor and an endplate with a centered hole formed by a metallic support tube. A cylindrical sample can be inserted into the cavity and further into the hollow center conductor through the endplate hole. Liquids, paste or powder samples must be contained in a sample holder, usually a glass tube. The hollow center conductor and the endplate hole will, in addition, provide a concentric alignment. The holes in the center conductor and endplate are so small compared with the wavelength that only evanescent modes exist even when the inserted sample has a relatively high dielectric constant, e.g., $\epsilon_r = 80$. Therefore, the fields will be strongly attenuated inside the holes, and so the geometrical discontinuities at the sample ends will not affect the cavity fields. If we assume that the fields vanish at the points, say, $z = H_1$ and $z = -H_2$ as shown in Fig. 1(b), an artificial metallic wall can be erected to simplify the analysis. The wall position, $H_1$ and $H_2$, is chosen based on the decaying rate of the field inside the holes which will be discussed later.

### B. Mode-Matching Formulation

The method of mode-matching has been employed for analyzing coaxial re-entrant cavities by several authors [7], [11]–[13] and is also selected in this paper for investigating the hole effects. The geometry shown in Fig. 1(a) can be divided into four subareas $A$, $B$, $C$, and $D$ as demonstrated in Fig. 1(b). According to the symmetry of the structure, an infinite number of axially symmetric modes (TM) can be assumed for field expansions in each subarea as follows

In subarea $A$:

$$E_z^A = \sum_{n=0}^{\infty} a_n Z_{0n}^A(k_n^A r) \cos \beta_n^A z \tag{1.1}$$

$$E_r^A = \sum_{n=1}^{\infty} a_n (\beta_n^A / k_n^A) Z_{1n}^A (k_n^A r) \sin \beta_n^A z \tag{1.2}$$

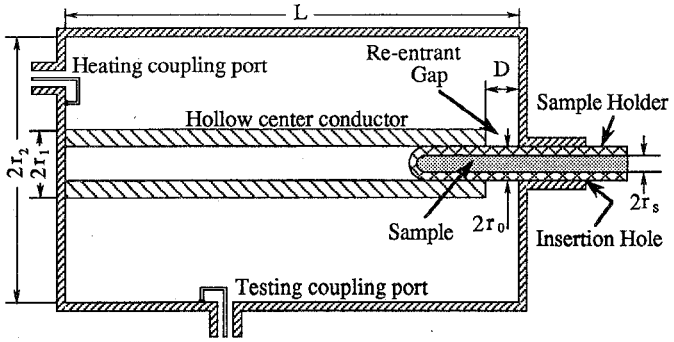


(a)

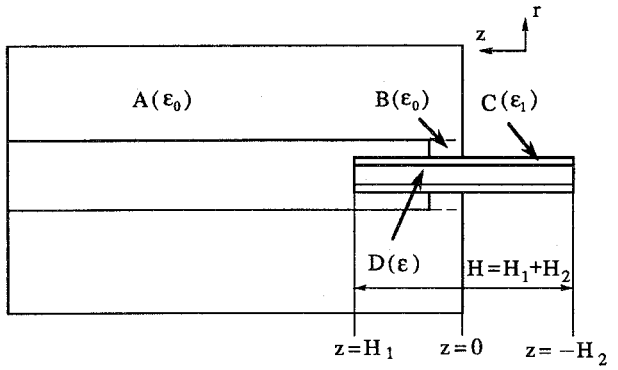


(b)

Fig. 1. The re-entrant coaxial cavity to be analyzed. (a) Cross section; (b) Subarea division for mode-matching analysis.

$$H_\phi^A = \sum_{n=0}^{\infty} a_n (j\omega\epsilon_0/k_n^A) Z_{1n}^A(k_n^A r) \cos \beta_n^A z \quad (1.3)$$

$$\beta_n^A = n\pi/L \quad (1.4)$$

$$(k_n^A)^2 = k_0^2 - (\beta_n^A)^2 \quad (1.5)$$

$$Z_{0n}^A(k_n^A r) = J_0(k_n^A r) - F_n^A Y_0(k_n^A r) \quad (1.6)$$

$$Z_{1n}^A(k_n^A r) = J_1(k_n^A r) - F_n^A Y_1(k_n^A r). \quad (1.7)$$

In subarea B:

$$E_z^B = \sum_{m=0}^{\infty} b_m Z_{0m}^B(k_m^B r) \cos \beta_m^B z \quad (2.1)$$

$$E_r^B = \sum_{m=1}^{\infty} b_m (\beta_m^B/k_m^B) Z_{1m}^B(k_m^B r) \sin \beta_m^B z \quad (2.2)$$

$$H_\phi^B = \sum_{m=0}^{\infty} b_m (j\omega\epsilon_0/k_m^B) Z_{1m}^B(k_m^B r) \cos \beta_m^B z \quad (2.3)$$

$$\beta_m^B = m\pi/D \quad (2.4)$$

$$(k_m^B)^2 = k_0^2 - (\beta_m^B)^2 \quad (2.5)$$

$$Z_{0m}^B(k_m^B r) = J_0(k_m^B r) - F_m^B Y_0(k_m^B r) \quad (2.6)$$

$$Z_{1m}^B(k_m^B r) = J_1(k_m^B r) - F_m^B Y_1(k_m^B r). \quad (2.7)$$

In subarea C:

$$E_z^C = \sum_{l=0}^{\infty} c_l Z_{0l}^C(k_l^C r) \cos \beta_l^C z \quad (3.1)$$

$$E_r^C = \sum_{l=1}^{\infty} c_l (\beta_l^C/k_l^C) Z_{1l}^C(k_l^C r) \sin \beta_l^C z \quad (3.2)$$

$$H_\phi^C = \sum_{l=0}^{\infty} c_l (j\omega\epsilon_0\epsilon_{r1}/k_l^C) Z_{1l}^C(k_l^C r) \cos \beta_l^C z \quad (3.3)$$

$$\beta_l^C = l\pi/H \quad (3.4)$$

$$(k_l^C)^2 = \epsilon_{r1} k_0^2 - (\beta_l^C)^2 \quad (3.5)$$

$$Z_{0l}^C(k_l^C r) = J_0(k_l^C r) - F_l^C Y_0(k_l^C r) \quad (3.6)$$

$$Z_{1l}^C(k_l^C r) = J_1(k_l^C r) - F_l^C Y_1(k_l^C r). \quad (3.7)$$

In subarea D:

$$E_z^D = \sum_{l=0}^{\infty} d_l J_0(k_l^D r) \cos \beta_l^D z \quad (4.1)$$

$$E_r^D = \sum_{l=1}^{\infty} d_l (\beta_l^D/k_l^D) J_1(k_l^D r) \sin \beta_l^D z \quad (4.2)$$

$$H_\phi^D = \sum_{l=0}^{\infty} d_l (j\omega\epsilon_0\epsilon_r/k_l^D) J_1(k_l^D r) \cos \beta_l^D z \quad (4.3)$$

$$\beta_l^D = \beta_l^C = l\pi/H \quad (4.4)$$

$$(k_l^D)^2 = \epsilon_r k_0^2 - (\beta_l^D)^2. \quad (4.5)$$

In the above field expansions, the following notation is used. Superscripts, $A$, $B$, $C$ and $D$ relate to each subarea; subscripts, $n$, $m$ and $l$ designate each mode integer; $a_n$, $b_m$, $c_l$ and $d_l$ are the expansion coefficients, i.e., mode amplitudes; $\beta$ is the axial wave number and $k$ is the transverse wave number; $Z_0$ and $Z_1$ are the combinational Bessel functions of the first and the second kind and $F$ is the associated constant which is determined by the boundary conditions.

The boundary conditions at the axial walls (assumed perfect conductors) at $z = 0$, $L$, $D$, $H_1$ and $-H_2$ have already been satisfied by using the axial mode function of $\{\sin \beta z\}$. The condition that $E_z^A = 0$ at $r = r_2$ requires

$$F_n^A = J_0(k_n^A r_2)/Y_0(k_n^A r_2). \quad (5)$$

Using the continuity of $E_z$ or $H_\phi$ at the common surface of subarea $C$ and $D$, i.e., $r = r_s$, we can determine $F_l^C$ and $d_l$ directly by taking advantage of the fact that the fields in $C$ and $D$ depend on the same axial mode functions:

$$F_l^C = [J_1(k_l^C r_s) - h_l J_0(k_l^C r_s)]/[Y_1(k_l^C r_s) - h_l Y_0(k_l^C r_s)] \quad (6.1)$$

$$h_l = (\epsilon_r k_l^C/\epsilon_{r1} k_l^D)[J_1(k_l^D r_s)/J_0(k_l^D r_s)] \quad (6.2)$$

$$d_l = [Z_{0l}^C(K_l^C r_s)/J_0(k_l^D r_s)] c_l. \quad (7)$$

The rest of the unknowns are mode amplitudes $a_n$, $b_m$ and $c_l$, and constants $F_m^B$, which can be solved through matching tangential components $E_z$ and $H_\phi$ at the common surfaces between $A$ and $B$, and $B$ and $C$. Since the field expansions in these subareas do not share the same axial mode function, the Fourier method is employed to obtain

the following matrix equations:

$$\mathbb{A} = \mathbb{P}\mathbb{B} \tag{8}$$

$$\mathbb{G}\mathbb{B} = 0 \tag{9}$$

$$\mathbb{C} = \mathbb{U}\mathbb{B} \tag{10}$$

$$\mathbb{T}\mathbb{B} = 0 \tag{11}$$

where,

$$\mathbb{A} = (a_0, a_1, \cdots, a_{N-1})^T;\ \mathbb{B} = (b_0, b_1, \cdots, b_{M-1})^T;$$
$$\mathbb{C} = (c_0, c_1, \cdots, c_{L-1})^T$$

$$\mathbb{P} = [p_{nm}]_{N\times M};\ \mathbb{G} = [g_{ij}]_{M\times M};\ \mathbb{U} = [u_{lm}]_{L\times M};$$
$$\mathbb{T} = [t_{ij}]_{M\times M}$$

In the derivation of (8)–(11), the infinite series of field expansions in subareas $A$, $B$ and $C$ are truncated after the $(N-1)$th, $(M-1)$th and $(L-1)$th term. The matrix elements $p_{nm}$, $g_{ij}$, $u_{lm}$ and $t_{ij}$ are functions only of geometry parameters and $\epsilon_r$ and $\epsilon_{r1}$ if the resonant frequency $f_0$ and constants $F_m^B$ are known.

### C. Numerical Methods

In the simplest case of absence of both the sample insertion hole and sample holder, i.e., $H_1 = H_2 = 0$ and $\epsilon_{r1} = 1$, we have $\mathbb{G} = \mathbb{B}$, $\mathbb{T} = 0$ and $F_m^B = F_m^C$. The problem is thus reduced to solving only (9). To avoid a trivial solution, it is required that

$$\det \mathbb{G} = 0. \tag{12}$$

The solution of this equation gives us the resonant frequency of the cavity without holes. With the known $f_0$ and assumed unity $b_0$, $b_m$ can be found by solving (9), from which, $a_n$ and $d_1$ can in turn be calculated simply by (8) and (7).

In the presence of sample insertion holes, $F_m^B$ cannot be expressed in an explicit form as $F_l^C$ in (6), but can be found along with the resonant frequency $f_0$ through solving (9) and (11) simultaneously. Since matrix elements $g_{ij}$ and $t_{ij}$ are nonlinear functions of $f_0$ and $F_m^B$, the problem is one of solving a set of nonlinear algebraic equations with 2M variables: $f_0$, $F_m^B$ $(m = 0, 1, \cdots, M-1)$ and $b_m (m = 1, 2, \cdots, M-1)$. However, this problem can also be defined as searching for $f_0$ and $F_m^B$ that not only satisfy (12) and

$$\det \mathbb{T} = 0 \tag{13}$$

but also gives an identical solution of $\mathbb{B}$ from (9) and (11), i.e.,

$$(b_m)_G = (b_m)_T. \tag{14}$$

From a practical point of view, we may be content with an approximate solution of (12)–(14), which can be obtained through a procedure of minimizing the following objective function:

$$\mathrm{Ob}\,(f_0, F_0^B, \cdots, F_{M-1}^B) = W_1|\det \mathbb{G}| + W_2|\det \mathbb{T}| + W_3 \sum_{m=1}^{M-1} |(b_m)_G - (b_m)_T| \tag{15}$$

where, $W_1$, $W_2$ and $W_3$ are weight factors which are adjusted during the calculation [14].

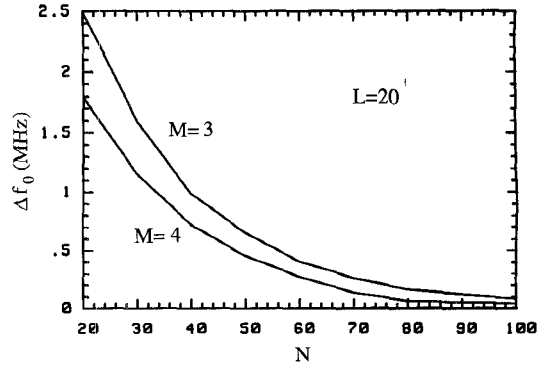


Fig. 2. The convergence rate of the calculation; $N$, $M$ and $L$ are the number of modes in subarea A, B and C (or D) which are preserved after the truncation; $r_0 = r_s = 0.25$, $r_1 = 1.25$, $r_2 = 4.5$, $L = 20.0$, $D = 0.5$, in cm, $\epsilon_r = 10.0$, $f_0 = 3070$ MHz.

TABLE I
CALCULATED RESONANT FREQUENCIES (MHz) AS COMPARED WITH MEASUREMENTS

| $D$ (CM) | $f_0$ (calc.) | $f_0$ (meas.) | $\Delta f_0/f_0$ (%) |
|---|---|---|---|
| 0.20 | 3040.3 | 3042.1 | −0.059 |
| 0.30 | 3052.2 | 3054.0 | −0.057 |
| 0.50 | 3072.0 | 3073.0 | −0.032 |
| 0.75 | 3091.2 | 3090.8 | +0.013 |
| 1.00 | 3106.8 | 3105.5 | +0.042 |

$r_0 = 0.355$, $r_1 = 1.244$, $r_2 = 5.0$, $L = 20.0$ cm, $\epsilon_r = 1$

Since the field expansions in subarea $B$ for a gap less than $\lambda/10$ are rapidly convergent series, $M$ can be as small as four. Due to a small number of variables, the simplex method [14], one of the direct minimizing methods, is chosen to search for $f_0$ and $F_m^B$ that minimize Ob. Based on this algorithm, a computer program is implemented to calculate the resonant frequencies, mode amplitudes of each subarea and the Q-factor of a given dielectric loaded cavity. It takes half a minute of CPU time on our Amdahl (5870) main frame if well-guessed initial values of $f_0$ and $F_m^B$ are entered. Fig. 2 exhibits the convergence rate of the calculation and shows that the calculation errors, which are mainly due to truncation errors, are within $\pm 0.1$ MHz at 3.0 GHz if $N > 50$. Moreover, calculated resonant frequencies of an empty cavity with varied gap widths are listed in Table I along with the measured values, which shows the discrepancy to be smaller than 0.06%. It should be mentioned that the error of frequency measurements may be as large as $\pm 0.5$ MHz for our scalar network analyzer (HP8756A) even after a one-hour warm-up and calibration against a microwave counter (EIP575).

## III. Hole Effects

The presence of the sample insertion hole in the re-entrant gap has similar effects on cavity characteristics as widening the gap. Using this analogy, we may qualitatively expect that the holes will cause the gap capacitance to decrease, or resonant frequency to increase, and the gap E-field to decrease. The reduced field will in turn lessen the dielectric sample loading effects [13], namely, the frequency shift and Q-factor drop due to the sample. All these effects are discussed in detail below based on the numerical calculations.

### A. Hole Field Attenuation

Due to the diameter of the holes being much less than the wavelength, fields cannot propagate but diminish along a path deeper into the holes. As shown in Fig. 3, the field, at some distance into the hole, is attenuated to, say 5% which corresponds to a negligible variation in the calculated resonant frequency. This distance, $z_h$, normalized by the hole diameter, may be called the effective depth of the hole. The effective depth will increase if a sample is introduced, in particular, a high permittivity sample. The dependence of the effective depth on a sample's dielectric constant is illustrated by the calculated results shown in Fig. 4. As expected, while the dielectric constant increases, the effective depth increases, and eventually reaches infinity where the hole no longer acts as a waveguide operating below cutoff. Moreover, the effective depth indicates the closest artificial wall position which one can use in the mode-matching analysis, namely, $H_1 = -H_2 \geq z_h$. This is then also the minimum sample length which one can use in practical measurements.

### B. Gap Field Distribution

As predicted, the E-field intensity in the re-entrant gap is weakened and its peak value no longer occurs on the axis when the holes are present adjacent to the gap. This is demonstrated in Fig. 5, where radial distributions of $E_z$ in the midplane of the re-entrant gap are plotted for three cavities: (1) without insertion holes or a sample holder; (2) with insertion holes but without the holder and (3) with both insertion holes and the holder. It shows that the peak field is shifted from the axis to the radial edge of the holes and that the presence of a sample holder reduces the gap field further.

### C. Resonant Frequency Shift

For the same cavity structures (1), (2) and (3) as shown in Fig. 5, resonant frequency shifts are calculated with varying dielectric constants and plotted in Fig. 6. The results are in qualitative agreement with those of the gap field in Fig. 5. In other words, the stronger the gap field, the greater the shift in resonant frequency. The slope of $\Delta f_0$ versus $\epsilon_r$ determines the sensitivity in dielectric determinations. However, it also commands the measurable range of dielectric properties because a larger detuning of a resonator tends to bring about more difficulties such as impedance mismatch in practical measurements. Therefore, a coaxial cavity with sample insertion holes and

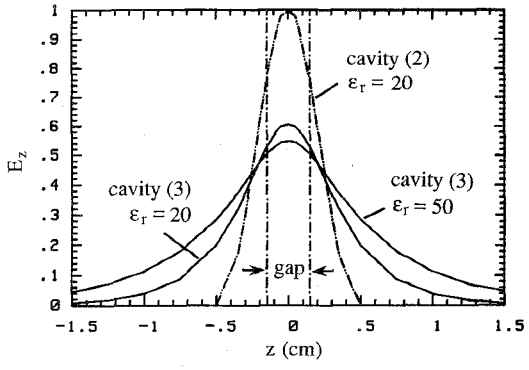


Fig. 3. The axial distribution of the normalized $E_z$ along $z$-axis (for cavity size, see Fig. 5).

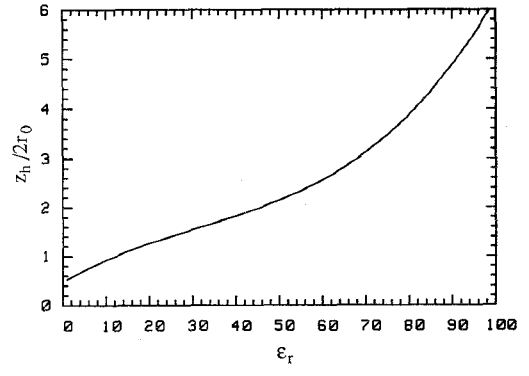


Fig. 4. The effective hole depth of cavity (3) (See Fig. 5) as a function of sample's dielectric constant at about 3 GHz.

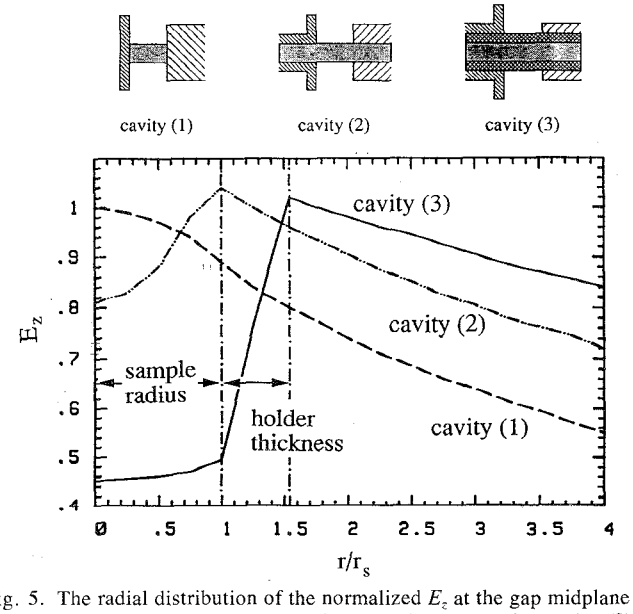


Fig. 5. The radial distribution of the normalized $E_z$ at the gap midplane at about 3 GHz; cavity (1)—without hole and holder ($r_0 = 0$), cavity (2)—with hole and without holder ($r_0 = r_s$), cavity (3)—with both hole and holder ($r_0 = 0.37$ cm, $\epsilon_{rh} = 3.78$); the rest cavity dimensions are identical, i.e. $r_s = 0.24$, $r_1 = 1.23$, $r_2 = 4.51$, $L = 20.5$, $D = 0.3$ cm.

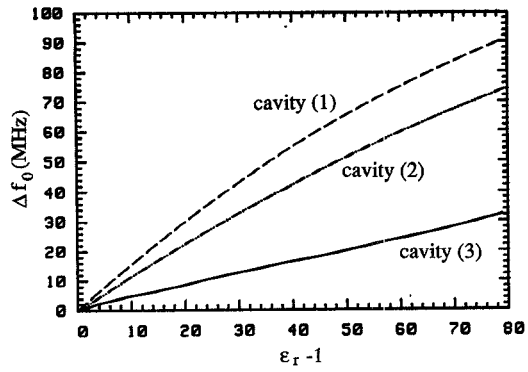


Fig. 6. Resonant frequency shift produced by a sample at about 3 GHz; cavity (1), (2) and (3) are the same as in Fig. 5.

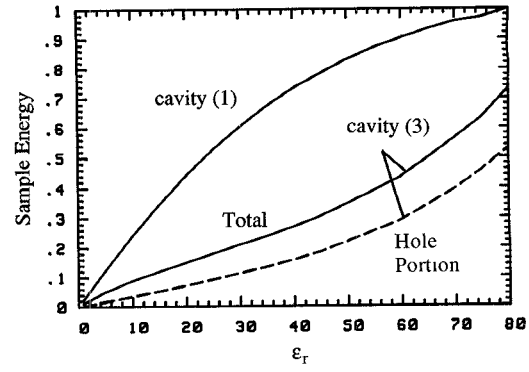


Fig. 7. Normalized electric energy stored in a sample, as a function of the sample's dielectric constant; for cavity (1) and (3), (see Fig. 5).

holder can extend the measurable range of dielectric properties. Moreover, it presents a better linearity of frequency shift as a function of dielectric constant. As shown in Fig. 6, the curve for cavity (3) is almost a straight line up to $\epsilon_r = 80$, which is a great convenience in dielectric determinations. This improvement in linearity is not only the consequence of a reduction of the gap field but also the outcome of an increased effective hole depth at a higher dielectric constant which offsets the saturation exhibited for a normal detuning curve, such as the curve for cavity (1) in Fig. 6.

### D. Energy Stored and Dissipated in Sample

The electric energy stored in a sample can be broken into two parts, namely, the gap portion energy and the hole portion energy. The presence of the holes reduces the gap portion energy because of the decreased gap field but also yields an additional energy in the holes. To examine these two portions of energy closely, the stored energy in a sample is integrated over the volume of the gap and the holes separately for varied dielectric constants, and the results are presented in Fig. 7 together with the results for the no-hole case. It shows that the hole portion contributes an appreciable percentage of the total energy stored in the sample, and that it increases with dielectric constant at an increasing rate. It is this hole portion energy that compensates for the reduction of the E-field in the sample due to the increase of the dielectric constant, thus extending the linear range in the curve of the resonant frequency shift versus dielectric constant.

According to the approximation of perturbation theory, the dissipated energy in the sample is directly proportional to the stored energy, with the constant of proportionality being the loss tangent of the sample. Consequently, for a constant loss tangent, the dissipated energy in the sample increases with the dielectric constant, $\epsilon_r$, in the same manner as the stored energy, i.e., at a nearly constant rate in the lower range of $\epsilon_r$ and at an increasing rate at higher $\epsilon_r$. When the cavity is loaded with a sample having both a high dielectric constant and a high loss tangent, it will present a very low Q-factor and will be severely under-coupled. Therefore, in order to obtain a wider measurement range, the sample volume must still be limited, even though the insertion hole already tends to lower the gap fields.

## IV. Dielectric Determination and Error Analysis

To determine dielectric constants and loss tangents, it is essential to find their relationships to the measurable parameters, which are the resonant frequency shift and the Q-factor change produced by the sample in case of cavity perturbation methods. Such relationships can be easily obtained by the mode-matching analysis in the form of calibration curves.

### A. Dielectric Constant and its Error

A calibration curve of dielectric constant is given in Fig. 8, corresponding to the geometry of our experimental cavity and the frequency band of interest. Using a least square fit, this curve can also be expressed by the polynomial

$$\epsilon_r = 1 + 1.56(\Delta f_0) + 0.071(\Delta f_0)^2 - 0.0014(\Delta f_0)^3 - 0.7 \times 10^{-6}(\Delta f_0)^4 + 0.11 \times 10^{-6}(\Delta f_0)^5 \quad (16)$$

where $\Delta f_0$ is the absolute value of the resonant frequency shift in MHz produced by a sample of permittivity, $\epsilon_r$. Thus, the dielectric constant can be readily determined, either graphically or mathematically, once the resonant frequency shift due to the inserted sample is measured.

If we initially neglect the error in the calibration curve, the uncertainty in the determined dielectric constant can be evaluated by

$$\delta \epsilon_r = \frac{d\epsilon_r}{d(\Delta f_0)} \delta (\Delta f_0) \quad (17)$$

where, $d\epsilon_r/d(\Delta f_0)$ is the slope of the dielectric calibration curve which is also plotted in Fig. 8 and $\delta(\Delta f_0)$ is the measurement error in the resonant frequency shift. Since $d\epsilon_r/d(\Delta f_0) \leq 2.8/\text{MHz}$ and $\delta(\Delta f_0) \leq 0.03$ MHz for, say an HP8350 Sweep Oscillator, $\delta \epsilon_r$ will not exceed $\pm 0.1$.

The errors in the calibration curve include numerical errors such as truncation errors and round-off errors, er-

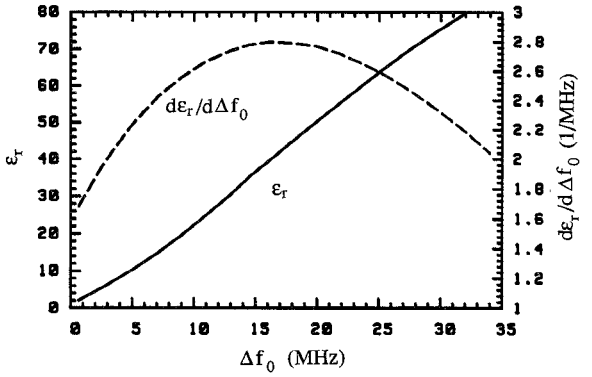


Fig. 8. Calibration curve for determining dielectric constant; $r_s = 0.24$, $r_0 = 0.355$, $r_1 = 1.244$, $r_2 = 5.0$, $L = 20.0$, $D = 0.3$ cm, $\epsilon_{rh} = 3.78$, $f_0 = 3.05$ GHz.

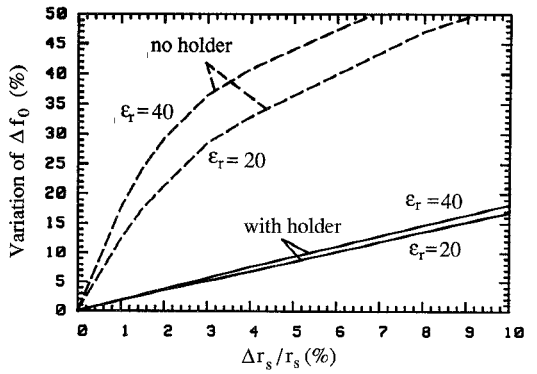


Fig. 9. The effect of varying sample radii on the resonant frequency shift; the cavity is the same as in Fig. 8.

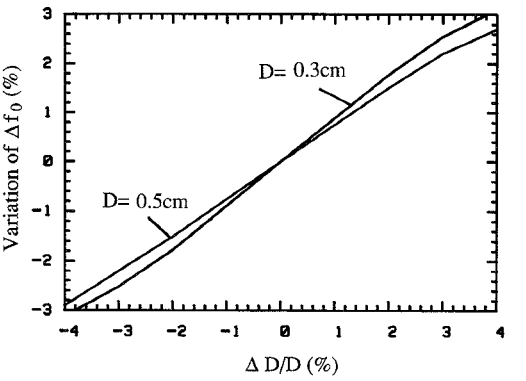


Fig. 10. The effect of varying gap widths on the resonant frequency shift; the cavity is the same as in Fig. 8.

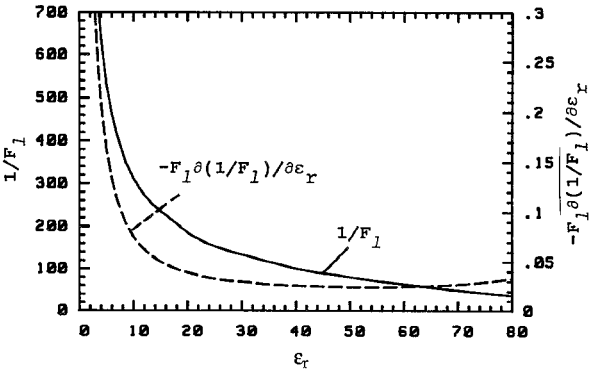


Fig. 11. Calibration curve for determining loss tangent; the cavity is identical to that in Fig. 8.

rors due to the uncertainties in cavity and sample dimensions: $r_s$, $r_0$, $r_1$, $r_2$, $L$ and $D$, and errors caused by the departures of a real cavity from the ideal mathematical model as caused by eccentricity of the sample placement, effects of the movable short circuit and coupling loop. Obviously, the use of the resonant frequency shift instead of the resonant frequency itself greatly reduces most of these errors. Furthermore, the structure with the sample insertion holes limits the eccentricity of sample placement and also eliminates completely the air gap problem which may cause an error of over 10% in $\epsilon_r$ [7].

Nevertheless, the error in the determined $\epsilon_r$ is more sensitive to the uncertainties in sample radius ($r_s$) and gap width ($D$) than in the other dimensions. Figs. 9 and 10 demonstrate the influences of variations in $r_s$ and $D$ on the calculated $\Delta f_0$, and in turn on $\epsilon_r$. From Fig. 9, it can be seen that if a sample holder is not used, even a slight looseness of the sample in the holes will produce a significant error in $\Delta f_0$, in the same way as the axial air gap in cavities without insertion holes. Fortunately, this error can be greatly suppressed by using a low permittivity sample holder such as a quartz tube ($\epsilon_{r1} = 3.78$). The error caused by a variation of $D$ is relatively small and will not exceed 1% if $\Delta D$ is controlled within 1%. It would be much larger if the cavity had no insertion hole and thus axial air gaps existed unavoidably at the sample ends. The results in Figs. 9 and 10 also show that 1) the error in $\Delta f_0$ will become larger for a higher dielectric constant sample and a narrower gap; 2) the error caused by the looseness of the sample and the sample holder may be compensated by using a slightly larger gap to keep the sample volume in the gap constant.

### B. Loss Tangent and its Error

The Q-factor of a dielectric loaded cavity can be expressed as

$$1/Q_L = 1/Q_C + 1/Q_D \tag{18}$$

where, $Q_C$ and $Q_D$ is the cavity Q-factor which accounts for the wall loss and the sample loss, respectively. By definition, $Q_D$ can be written as

$$1/Q_D = F_l \tan \delta \tag{19}$$

$$F_l = W_D/W_C \tag{20}$$

where, $W_C$ and $W_D$ is the electric energy stored in the whole cavity and in the sample respectively, and $F_l$ is their ratio which represents the degree of sample loading to a cavity and is called sample loading factor. From (18) and (19), the loss tangent can be found by

$$\tan \delta = (1/Q_L - 1/Q_C)/F_l$$
$$\approx (1/Q_L - 1/Q_0)/F_l = \Delta(1/Q)/F_l \tag{21}$$

$Q_0$ is the unloaded cavity Q-factor and it, together with $Q_L$, can be obtained from measurements. In Fig. 11 is plotted the calibration curve of loss tangent, i.e., $1/F_l$,

TABLE II
EXPERIMENTAL RESULTS OF DIELECTRIC PROPERTIES AS COMPARED WITH PUBLISHED DATA ($f$ = 3.05 GHz, $T$ = 23°C)

| Sample | Present Work | | | | Reference Data | | |
|---|---|---|---|---|---|---|---|
| | $\epsilon_r$ | $\Delta\epsilon_r$ | tan $\delta$ | $\Delta$ tan $\delta$ | $\epsilon_r$ | tan $\delta$ | |
| Teflon | 1.94 | +0.08 | 0.0025 | +0.0006 | 2.05 | 0.0083 | (1) |
| | | −1.16 | | −0.0006 | 2.10 | 0.0002 | (2) |
| Nylon | 2.94 | +0.07 | 0.010 | +0.0026 | 3.04 | 0.012 | (2) |
| | | −0.19 | | −0.0022 | | | |
| Quartz | 3.74 | +0.06 | 0.0005 | +0.00012 | 3.78 | 0.0005 | (3) |
| (Corning) | | −0.20 | | −0.0001 | | | |
| Soda Lime | 6.45 | +0.04 | 0.012 | +0.0034 | 6.71 | 0.013 | (2) |
| (0080, Corning) | | −0.28 | | −0.0024 | | | |
| Alumina | 8.70 | +0.03 | 0.0008 | +0.00012 | 9.30 | 0.0002 | (4) |
| (Al-23, JM) | | −0.36 | | −0.0001 | | | |
| CuO | 3.44 | +0.05 | 0.247 | +0.037 | 3.20 | 0.28 | (5) |
| (powder, 2.70 g/cc) | | −0.20 | | −0.025 | | | |
| Benzene | 2.24 | +0.04 | 0.0040 | ±0.001 | 2.28 | ≤0.002 | (6) |
| | | −0.12 | | | | | |
| Monochlorobenzene | 5.39 | +0.05 | 0.110 | +0.024 | 5.54 | 0.12 | (7) |
| | | −0.15 | | −0.022 | | | |
| Methanol | 19.9 | +0.30 | 0.744 | ±0.15 | 18.9 | 0.75 | (8) |
| | | | | | 21.0 | 0.62 | (2) |
| Distilled Water | 76.5 | −1.2 | 0.153 | +0.035 | 77.3 | 0.155 | (2) |
| | | | | −0.030 | | | |
| 0.1M NaCl | 73.3 | −1.2 | 0.219 | +0.05 | 75.2 | 0.225 | (9) |
| | | | | −0.04 | | | |
| 10%A, 20%M and | 6.66 | +0.03 | 0.278 | +0.061 | 7.3 | 0.22 | (7) |
| 70%B | | −0.20 | | −0.056 | | | |
| 40%W and 60%M | 45.9 | −0.69 | 0.426 | +0.094 | 46.0 | 0.37 | (7) |
| | | | | −0.085 | | | |

A-Acetone, M-Methanol, B-Benzene, W-Distilled Water

(1) HP Product Note 8510-3, Aug. 1985
(2) A. R. von Hippel, Dielectric Materials and Application, MIT Press, 1954
(3) A. C. Metaxas, et al, Industrial Microwave Heating, IEE England, UK, 1988
(4) Data from Superior Technical Ceramics Corp., St. Albans, VT, U.S.A.
(5) W. R. Tinga, Electromagnetic Energy Reviews, vol. 1, p. 47, 1988
(6) B. Terselius, *et al.*, J. of Microwave Power, 13(4), p. 327, 1978
(7) P. O. Risman, *et al.*, J. of Microwave Power, 6(2), p. 101, 1971
(8) B. P. Jordan, *et al.*, J. Phys. D: Appl. Phys., vol. 11, p. 695, 1978
(9) A. Stogryn, IEEE TRANS. *Microwave Theory Tech.* vol. MTT-19, p. 733, Aug. 1971

which, from (21), is equal to the loss tangent if $\Delta(1/Q) = 1$, as a function of $\epsilon_r$. This curve corresponds to the same cavity as the calibration curve of dielectric constant. As before, this curve can also be expressed by

$$1/F_l = 2101/\epsilon_r + 127 - 2.77\epsilon_r + 0.0253\epsilon_r^2. \quad (22)$$

Therefore, the loss tangent can be readily found if the $Q$ change is measured and the dielectric constant is known. The error involved in the thus determined loss tangent is estimated as follows.

Taking the variation of (21) and dividing it by tan $\delta$, we have

$$\frac{\delta(\tan\delta)}{\tan\delta} = \frac{\delta(\Delta(1/Q))}{\Delta(1/Q)} + F_l\delta(1/F_l) \quad (23)$$

which means that the relative error in tan $\delta$ is broken into two parts, the part due to the $Q$-measurement error

$$\frac{\delta(\Delta(1/Q))}{\Delta(1/Q)} = \frac{Q_L^2\delta Q_0 - Q_0^2\delta Q_L}{Q_L Q_0(Q_0 - Q_L)} \quad (24)$$

and the part due to the error in dielectric constant transferred through the filling factor

$$F_l\delta(1/F_l) = F_l(\partial(1/F_l)/\partial\epsilon_r)\cdot\delta\epsilon_r \quad (25)$$

If the approximation is made that $\delta Q_0 = \delta Q_L = \delta Q$ and $(Q_L + Q_0)/(Q_L Q_0) = 2/Q$, (25) becomes

$$\delta(\Delta(1/Q))/(\Delta(1/Q) = -2\delta Q/Q \quad (26)$$

where $\delta Q/Q$ can be treated as the average relative error in $Q$ measurements. In our calibrated scalar reflectometer setup, such an error is mainly caused by the directivity of the dual directional coupler and is estimated to be ±10% for a 30 dB directivity and ±4% for a 40 dB directivity in the worst case [15].

The term of $F_l(\partial(1/F_l)/\partial\epsilon_r)$ is also plotted in Fig. 11. From before, $|\delta\epsilon_r| \leq 0.1$, so that the tan $\delta$ error from $\epsilon_r$ is negligible if $\epsilon_r \geq 10$. However, this error will rise to 8% when $\epsilon_r$ is close to unity.

## V. EXPERIMENTAL MEASUREMENTS

It has been shown that the dielectric constant and loss tangent of a sample can be determined from two theoretical calibration curves if one can measure the resonant frequency and Q-factor before and after the sample is inserted. In this work, a scalar network analyzer (HP8756A) is utilized in a reflectometer setup [16] to measure the reflection spectrum, from which the resonant frequency and Q-factor are found.

A number of different samples were measured with the coaxial cavity analyzed above and their dielectric properties were determined using the calibration curves in Figs. 8 and 11. The results and their maximum error ranges are presented, together with the published data, in Table II.

The $\Delta\epsilon_r$ in Table II is estimated by considering the error in measured $\Delta f_0$ and the error due to the looseness of the test tube and samples. The former causes a maximum error of $\pm 0.1\%$ in $\epsilon_r$; the latter is equivalent to a sample radius variation of $-0.5\%$ to $-1.0\%$ and $-1.0\%$ to $-1.5\%$ which results in a maximum relative error of $-1\%$ to $-1.5\%$ and $-1\%$ to $-3\%$ in $\epsilon_r$ for liquid and solid samples respectively. The errors in loss tangent are mainly caused by the inaccuracy of $Q$ measurements which is $\pm 10\%$ for the worst case in our experimental setup. The inaccuracy of $\epsilon_r$, although to a lesser degree, also implicitly affects the accuracy of loss tangent as seen in (25).

The method of dielectric measurement presented is based on the calculated calibration curves. In this sense, it is an absolute method which does not rely on the reference data. Nevertheless, it still gives results in good agreement with the reference data as shown in Table II.

## VI. Summary

A coaxial re-entrant cavity with composite sample insertion holes is analyzed using a four-subarea mode-matching formulation. The numerical results reveal that the hole presence leads not only to a reduction of the gap field but also to an energy storage inside the holes. These hole effects result in a nearly linear function of the resonant frequency shift for varying dielectric constants.

Two calibration curves for determining the dielectric constant and loss factor are derived from theoretical calculations rather than from experimental measurements. Nonetheless, the dielectric data obtained from such an absolute method are still in good agreement with the published data. The error analysis show that the accuracy can be improved further if the measurement errors in the resonant frequency and Q-factor are reduced.

## References


[1] W. R. Tinga, B. Q. Tian, and W. A. G. Voss, "New high temperature multipurpose applicator," *Mat. Res. Soc. Proc.*, vol. 189, pp. 111–116, 1991.

[2] Weiguo Xi and W. R. Tinga, "High temperature microwave dielectrometer," *Amer. Cer. Soc., Ceramic Trans.*, vol. 21, "Microwave: Theory and Applications in Materials Processing," pp. 647–654, 1991.

[3] F. Horner, T. A. Taylor, R. Dunsmuir, J. Lamb, and W. Jackson, "Resonance methods of dielectric measurement at centimeter wavelengths," *Proc. Inst. Elec. Eng.*, vol. 93, pt. III, pp. 53–68, 1946.

[4] G. Roussy and M. Felden, "A sensitive method for measuring complex permittivity with a microwave resonator," *IEEE Trans. Microwave Theory Tech.*, vol. 14, pp. 171–175, Apr. 1966.

[5] A. W. Kraszewski and S. O. Nelson, "Use of a microwave cavity for sensing dielectric properties of arbitrarily shaped biological objects," *IEEE Trans. Microwave Theory Tech.*, vol. 38, pp. 858–863, July 1990.

[6] K. S. Champlin and G. H. Glover, "Influence of waveguide contact on measured complex permittivity of semiconductors," *J. Appl. Phys.*, vol. 37, no. 6, pp. 2355–2360, 1966.

[7] A. Kaczkowski and A. Milewski, "High-accuracy wide-range measurement method for determination of complex permittivity in re-entrant cavity: Part A and B," *IEEE Trans. Microwave Theory Tech.*, vol. 28, pp. 225–231, Mar. 1980.

[8] A. J. Estin and H. E. Bussey, "Errors in dielectric measurements due to a sample insertion hole in a cavity," *IRE Trans. Microwave Theory Tech.*, vol. 8, pp. 650–653, Nov. 1960.

[9] S. Li, C. Akyel and R. G. Bosisio, "Precise calculations and measurements on the complex dielectric constant of lossy materials using $TM_{010}$ cavity perturbation techniques," *IEEE Trans. Microwave Theory Tech.*, vol. 29, pp. 1044–1047, Oct. 1981.

[10] S. Gauthier, L. Marchildon, and C. Akyel, "Shift of the complex frequency of a dielectric loaded cavity produced by small sample insertion holes," *IEEE Trans. Microwave Theory Tech.*, vol. 37, pp. 801–804, Apr. 1989.

[11] O. V. Karpova, "On an absolute method of measurement of dielectric properties of a solid using a $\pi$-shaped resonator," *Fiz. Twerd. Tela*, vol. 1, pp. 246–255, Feb. 1959.

[12] A. Milewski, "Coaxial lumped capacitance resonators for the investigations of dielectrics," *Electron Tech.*, vol. 10, pp. 71–98, Jan. 1977.

[13] Weiguo Xi, W. R. Tinga, W. A. G. Voss, and B. Q. Tian, "New results for coaxial re-entrant cavity with partially dielectric filled gap," IEEE Trans. Microwave Theory Tech., vol. 40, pp. 747–753, Apr. 1992.

[14] A. Ralston and H. S. Wilf, *Mathematical Methods for Digital Computers*. Vol. II. New York: Wiley, 1968.

[15] W. R. Tinga and W. Xi, "Reflectometer Q-factor measurements and errors," Internal Lab Report, Microwave Power Lab, University of Alberta, Edmonton, AB, Canada, 1991.

[16] C. G. Montgomery, *Technique of Microwave Measurements*. New York: McGraw-Hill, 1947.



**Weiguo Xi** was born in Jiangsu, China in 1959. He received the B.Sc. (1982) and the M.Sc. (1985) degrees in Electronic Engineering from Southeast University (former Nanjing Institute of Technology).

He then joined the Electronics Research Institute of Southeast University, working as a researcher and lecturer in the theory of electron optics and the design of electron guns until 1989. Since then, he has been working towards a Ph.D degree in electrical engineering at the University of Alberta, Edmonton AB, Canada. His current research interests include dielectric measurements, microwave heating and numerical analysis of microwave resonators.


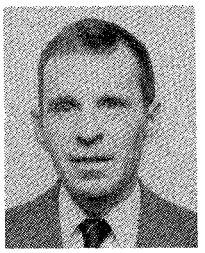


**Wayne R. Tinga** (S'62–M'68) received the Ph.D. degree in electrical engineering in 1969 from the University of Alberta, Edmonton, AB, Canada where he became assistant professor in 1970, associate professor in 1974 and full professor in 1980. He was on leave with Litton Microwave Cooking R/D Labs from 1979-1980 where he worked on developing one of his patents on frequency agile computer controlled microwave ovens.

He is a Fellow in the International Microwave Power Institute (IMPI) and served IMPI in many capacities since its inception in 1966 as President, Board Chairman, Executive Director, Symposium Chairman, and Technical Program Co-chairman. He also served on many technical committees dealing with Frequency Allocations, Radio Frequency Interference and Safety Standards. In addition, he served as Associate Editor of the *Journal of Microwave Power* (1970–1978), its Editorial Review Board (1978-present), and is on the review board of IEEE TRANSACTIONS ON Geoscience AND REMOTE SENSING (1988–1991). From 1983–1986, he was on leave to Dordt College, Sioux Center, IA, where he put in place a 4-year electrical engineering program. After his return to the University of Alberta, he was acting Director of Computer Engineering (1987–1988).

Dr. Tinga is a member of the Professional Engineering Association of Alberta, IMPI, the American Ceramics Society and the Materials Research Society. He has published over 60 technical papers and co-authored a number of tutorial books on microwave power. Currently, he is pursuing research in the area of high temperature dielectric measurement methods and modelling.